



ORIGINAL ARTICLE

Enhanced degradation of quinoline in three-dimensional electro-Fenton system through NiCo₂S₄/g-C₃N₄ particles



Jun Chen^{a,1,*}, Boding Zhang^{a,1}, Bingxing Wang^a, Chengxing Cui^a, Songlin Wang^a, Jichao Wang^a, Wenlong Zhang^{a,b}

^a College of Chemistry and Chemical Engineering, Henan Institute of Science and Technology, Xinxiang 453003, China

^b College of Chemistry, Zhengzhou University, Zhengzhou 450001, China

Received 16 February 2023; accepted 8 May 2023

Available online 12 May 2023

KEYWORDS

Electro-Fenton;
Catalytic;
Particle electrodes;
Hydroxyl radicals;
Degradation

Abstract The stability and toxicity of quinolines are difficult to degrade by conventional physicochemical and biological methods, posing a threat to human health and the environment. In this study, we prepared NiCo₂S₄/g-C₃N₄ particles and applied them in an electrochemical reactor to form a three-dimensional catalytic particle electro-Fenton system (3D-EF), which can efficiently remove quinoline from wastewater. The NiCo₂S₄/g-C₃N₄ catalytic particles were characterized by XRD, SEM, TEM, XPS. The optimum conditions for 3D-EF were 30 min reaction time, 60 g/L NiCo₂S₄/g-C₃N₄ particles dosage, pH value of 3, 67.6 mmol/L H₂O₂ concentration, 12.1 ms/cm conductivity and 5 A current. Under the optimum conditions, a chemical oxygen demand (COD) removal rate of 95.6% was achieved. NiCo₂S₄/g-C₃N₄ catalytic particles can be easily recovered by filtration and can be reused. Kinetic analysis showed that the COD degradation of quinoline solutions by the 3D-EF followed a first-order kinetic model. To determine the important role of hydroxyl radicals in the electrochemical process, electron paramagnetic reaction (EPR) and radical scavenging experiments were performed. Finally, in order to elucidate the degradation mechanism, the intermediates were identified by high performance liquid chromatography-mass spectrometry (HPLC-MS) and two possible degradation pathways were proposed. Meanwhile, the biochemical analysis of quinoline wastewater was also performed.

© 2023 Published by Elsevier B.V. on behalf of King Saud University. This is an open access article under the CC BY-NC-ND license (<http://creativecommons.org/licenses/by-nc-nd/4.0/>).

* Corresponding author at: College of Chemistry and Chemical Engineering, Henan Institute of Science and Technology, Xinxiang 453003, China.

E-mail addresses: junchen713@126.com (J. Chen), zhangboding2022@126.com (B. Zhang), wangbxucl@outlook.com (B. Wang), chengxing-cui@hist.edu (C. Cui), wangsonglin2009@163.com (S. Wang), wangjichao@hist.edu (J. Wang), zzuzhangwenlong@163.com (W. Zhang).

¹ Co-first authors. They contributed equally to this work.

1. Introduction

Quinoline is a typical nitrogen-containing heterocyclic compound, which is an important raw material for various artificial compounds such as drugs, dyes, solvents, preservatives and disinfectants (Luo et al., 2020). At the same time, due to the larger polarity and higher solubility, it is more likely to exist in the aqueous environment, such as coking wastewater, rubber wastewater and petroleum wastewater. Most nitrogen-containing heterocyclic compounds are toxic, mutagenic and carcinogenic, difficult to biodegrade and incompletely degraded in actual wastewater, posing a great threat to the ecological environment and human health (Zhao et al., 2021). Therefore, a simple and efficient technology is needed to solve the quinoline wastewater.

Advanced oxidation processes that converts difficult to degrade complex organic pollutants into small molecules by generating free radicals ($\cdot\text{OH}$, $\cdot\text{SO}_4$) with oxidizing power (Long et al., 2018). Ozone oxidation (Yuan et al., 2023), photocatalysis (Masekela et al., 2023), and catalytic wet air are all advanced oxidation processes, but the low removal efficiency, complex operating conditions, and high cost of industrial applications of these methods have limited their development in the treatment of wastewater. Electrocatalytic has the characteristics of energy-saving and time-saving, long life, stable performance and multi-functionality, which is gradually attracted people's attention (Liu et al., 2021). The three-dimensional electrode catalytic oxidation has received increasing attention in recent years, and it is just an extension and upgrade of electrocatalysis. Three-dimensional electrode catalytic oxidation is a technique in which particles are filled between the main electrode plates to form a three-dimensional electrode in a conventional electrolyzer, and electrochemical reactions occur on the surface of the particle electrodes to degrade organic matter (Hong et al., 2021, Chen et al., 2022b). The three-dimensional electrode catalytic oxidation is mainly used to treat wastewater by coupling the electrocatalytic with the three-dimensional electrode method, which can simultaneously carry out direct anodic oxidation, cathodic reduction to produce H_2O_2 , Fenton reaction catalyzed by Fe^{2+} , $\cdot\text{OH}$ indirect oxidation, particle electrode adsorption, particle electrode catalytic oxidation (Zhang et al., 2018a, Hou et al., 2017, Li et al., 2021a). It is an electrochemical oxidation technology that combines multiple effects. In this technique, the choice of particle electrodes is crucial.

Metal sulfides are not only the main materials for lithium-ion batteries and supercapacitors due to their high electrical conductivity and good thermal stability, but also are widely used as bifunctional catalysts for hydrogen and oxygen evolution (Barhoumi et al., 2017, Chen et al., 2019). In recent years, it has been shown that metal sulphides can have many positive effects in the wastewater treatment process. Xu et al. performed Fenton-like catalytic degradation of rhodamine wastewater by preparing Co_9S_8 nanocrystals with a removal efficiency of 100% in 14 min (Xu et al., 2021). In a recent study by Lin et al. a small amount of Fe_3S_4 was used as a catalyst to remove 95% of the BPA within 120 min (Lin et al., 2019). Poly-metallic doping can further enhance the catalytic activity of sulphides (Li et al., 2021b). Transition metals, such as Fe, Cu, Co, Ni and Mn, are essentially excellent activators of oxidants in homogeneous or non-homogeneous reactions (Feng et al., 2018). Among them, Co is recognised as one of the best activators. Its catalytic properties are comparable to those of precious metals (Chen et al., 2020). It is able to coordinate with surface oxygen-containing groups to create new active sites and enhance surface charge transport on the material (Song et al., 2019). In addition, intentional doping with Co can reduce the local functional density and protect the specific sub-stable structure from damage in strong oxidizing environments (Chaugule et al., 2019). Ni can be effectively used for the catalytic decomposition of organic pollutants due to its environmental friendliness, unique magnetic properties, high electron donating ability and cost effectiveness (Bhaumik et al., 2022). The incorporation of transition metal elements such as Co and Ni can significantly increase the number of effective active sites

and further improve the catalytic activity of the wastewater treatment. Finally, the choice of catalyst carrier is a key step in the successful preparation of the particle electrode. $\text{g-C}_3\text{N}_4$ is stable, non-toxic and non-polluting and is often used as an environmentally friendly catalyst or catalyst carrier for pollutant degradation, CO_2 reduction and hydrogen separation reactions (Jiang et al., 2015). In addition, the $\text{g-C}_3\text{N}_4$ surface can provide lone pairs of electrons to trap transition metal ions, forming a tight heterojunction interface and thus reducing the leaching of metal ions (Wang et al., 2021). Considering the synergistic effect between Co ions and Ni ions, the stable physicochemical properties of $\text{g-C}_3\text{N}_4$, and electron effects between sulfur element and transition metals, we expect that CoNiS -modified $\text{g-C}_3\text{N}_4$ ($\text{NiCo}_2\text{S}_4/\text{g-C}_3\text{N}_4$) can be used as a Fenton-like catalyst for the degradation of organic pollutants.

In this work, we synthesised $\text{NiCo}_2\text{S}_4/\text{g-C}_3\text{N}_4$ composites as catalytic particle electrodes. The catalytic particle electrodes were filled in an electrolytic cell composed of stainless steel plates to form a three-dimensional electro-Fenton system (3D-EF). The catalytic particle electrodes were physicochemically characterized by XRD, SEM, TEM, and XPS. The degradation ability of $\text{CoNi}_2\text{S}_4/\text{g-C}_3\text{N}_4$ catalytic particle electrodes on quinoline wastewater under different conditions was investigated. The basic degradation mechanisms of the systems developed are described in detail. Finally, possible mineralisation pathways are proposed based on high performance liquid chromatography detection.

2. Material and methods

2.1. Reagents

Nickel chloride hexahydrate ($\text{NiCl}_2\cdot 6\text{H}_2\text{O}$), Cobaltous chloride hexahydrate ($\text{CoCl}_2\cdot 6\text{H}_2\text{O}$), urea ($\text{CH}_4\text{N}_2\text{O}$), sodium sulphide ($\text{Na}_2\text{S}\cdot 6\text{H}_2\text{O}$), quinoline, *tert*-butanol (C_4HO_{10}), sodium hydroxide (NaOH), sulphuric acid (H_2SO_4), melamine ($\text{C}_3\text{H}_6\text{N}_6$), Ethanol (EtOH) and graphite powder were obtained from Shanghai Macklin Biochemical Co., Ltd. All chemicals were not further purified.

2.2. Preparation of catalysts

Firstly, 100 g of melamine was packed into a 200 ml crucible and calcined in a muffle furnace at a temperature increase of $10\text{ }^\circ\text{C}/\text{min}$ for 2 h at $550\text{ }^\circ\text{C}$. After cooling to room temperature, a lump of yellow $\text{g-C}_3\text{N}_4$ was obtained and then ground into a powder (Molaei and Rahimi-Moghadam, 2021). Secondly, 1 mmol $\text{NiCl}_2\cdot 6\text{H}_2\text{O}$, 2 mmol $\text{CoCl}_2\cdot 6\text{H}_2\text{O}$ and 10 mmol urea were dissolved in 30 ml deionized water. The mixed solution was stirred for 30 min on a magnetic stirrer. The mixed solution was then put into Teflon-lined stainless-steel autoclaves to react at $180\text{ }^\circ\text{C}$ for 12 h to obtain the pink product was nickel-cobalt bimetallic hydroxide (NC-LDH). The obtained sample was washed with deionized water and ethanol for 3 times, and dried in a vacuum drying oven at $60\text{ }^\circ\text{C}$ for 12 h. Thirdly, NC-LDH was selected as the precursor for sulfidation. 0.0609 g of the dried NC-LDH precursor was dissolved into 30 ml of deionized water and stirred for 30 min to prepare a mixed solution. Added 0.4 g $\text{Na}_2\text{S}\cdot 6\text{H}_2\text{O}$ to the mixed solution and stirred evenly for 30 min. The final mixed brown solution in an Teflon-lined stainless-steel autoclaves to react at $160\text{ }^\circ\text{C}$ for 10 h. The black precipitate was washed by centrifugation with deionised water and ethanol for 3 times, and finally dried in a vacuum drying oven at $60\text{ }^\circ\text{C}$ for 12 h to obtain the black product CoNi_2S_4 . Finally, CoNi_2S_4 , $\text{g-C}_3\text{N}_4$,

graphite powder, asphalt and NH_4HCO_3 with a mass percentage of 15%, 60%, 10%, 14% and 1% were mixed and granulated evenly. Graphite powder was used as a filler to increase the electrical conductivity, asphalt as a high temperature binder and NH_4HCO_3 as a pore-forming agent to increase the specific surface area of the particle electrodes. The particles were calcined up to 500 °C at 5 °C/min in a vacuum tube furnace and then to obtain the black columnar particles $\text{NiCo}_2\text{S}_4/\text{g-C}_3\text{N}_4$.

2.3. Experimental setup

As shown in Fig. 1, the electrochemical unit consists mainly of: (1) A high frequency pulsed switching power supply. (2) A cathode and anode plate made of stainless steel with a spacing of 5 cm and the effective area of each electrode plate was 8 cm × 15 cm. (3) An electrochemical reactor with a volume of 1.5L made from polypropylene material. (4) Particle electrodes filled between the two electrode plates form the third pole under the action of an electric field. (5) Air was injected into the unit via a micro-porous aerator.

2.4. Characterization techniques

The compositional data of $\text{NiCo}_2\text{S}_4/\text{g-C}_3\text{N}_4$ particles was characterized using X-ray diffraction (XRD, D8-Advance, Bruker, Germany) by $\text{Cu K}\alpha$ radiation at a 2θ range of 10–80° with a scan speed of 4° min^{-1} . The scanning electron microscopy (SEM, Quanta 200, FEI, America) coupled with transmission electron microscopy (TEM, JEM-2100F, JEOL, Japan) was employed to identify the microscopic images and textural properties of the particles. The valence states of the constituent elements of $\text{NiCo}_2\text{S}_4/\text{g-C}_3\text{N}_4$ particles was measured by X-ray photoelectron spectroscopy (XPS, Kratos Axis Ultra DLD, SHIMADZU, Japan). XPS were carried out using unmonochromatized Al K α line at 1486.6 eV (12 kV with 20 mA anode current) and a Leybold EA-11 analyzer with constant pass energy of 100 eV.

2.5. Electrolysis tests

In this study, quinoline was added to deionised water and then stirred for 30 min to obtain a quinoline solution (1.5 g/L). The particle electrodes were placed in simulated wastewater for 6 h to eliminate the effect of adsorption on the test results. Stainless steel plates were placed parallel to each other on both sides of the electrochemical reactor, and then wastewater was added and connected to the power supply. It is also filled with a certain number of catalytic particles electrodes between the electrode plates. The pH and conductivity of the reaction solution was adjusted by the addition of H_2SO_4 and NaCl. During the experiments, the organic concentration in the wastewater was determined by the potassium dichromate method, and the COD removal rate was used to evaluate the degradation efficiency of the particle electrode. The experiments were conducted with stainless steel plates as the anode and cathode and $\text{NiCo}_2\text{S}_4/\text{g-C}_3\text{N}_4$ as the catalytic particle electrode. The three-dimensional electro-Fenton method (3D-EF) was used to treat quinoline solution with an initial COD of 3000 mg/L. The effects of electrolysis time (10–60 min), particles dosage (30–70 g/L), initial pH (2–6), H_2O_2 concentration

(19.4–96.4 mmol/L), conductivity (6.2–18.7 ms/cm) and current (2–6 A) on the COD removal of quinoline solution were investigated by the single-factor method.

2.6. Analytical test methods

The value of pH and conductivity in the solutions were measured with pH meter (PHSJ-4F, Shanghai Shanghai Yidian Scientific Instrument Co., Ltd, China) and conductivity meter (DDS-307A, Shanghai Yidian Scientific Instrument Co., Ltd, China), respectively. Chemical oxygen demand (COD) was directly measured using COD rapid tester (5B-3B, Beijing Lianhua Co., Ltd, China). Electron paramagnetic resonance (EPR, A300, Bruker, Germany) experiments were carried out identify free radicals in solutions, with 5,5-dimethyl-1-pyrroline-N-oxide (DMPO) as the spin-trapping agent. The degradation or transformation intermediates were analyzed using high performance liquid chromatography (HPLC, 1290, Agilent, America) and quadrupole time-of-flight mass spectrometry (Q-TOF-MS, 6530, Agilent, America).

The intermediate products were analyzed by HPLC with a TC-C18 column in positive ion mode. The HPLC-MS intermediate analysis is as follows: column temperature, 40 °C; mobile phase: (A) H_2O , (B) methanol A:B = 40:50 (V/V); flow rate, 1 ml/min; injection volume, 1.0 μL ; drying gas temperature, 300 °C; drying gas flow rate, 8 L/min; nebulizer gas pressure, 35 psi; sheath gas temperature, 300 °C; sheath gas flow rate, 11 L/min; capillary voltage, 3500 V.

3. Results and discussion

3.1. Characterization of catalyst

Fig. 2(a) shows the XRD spectra of NiCo_2S_4 , $\text{g-C}_3\text{N}_4$ and $\text{NiCo}_2\text{S}_4/\text{g-C}_3\text{N}_4$. The diffraction peaks at around 16.3°, 26.7°, 31.5°, 38.1°, 47.1°, 50.5°, 55.2° can be indexed as the (111), (220), (311), (400), (422), (511) and (440) planes of the standard card of NiCo_2S_4 (PDF 43-1477) (Su et al., 2022). $\text{g-C}_3\text{N}_4$ has a strong (002) diffraction peak near 27.6 °C, corresponding to the diffraction peak of the conjugated aromatic unit in the interlayer stacking; a weak (100) characteristic peak appears at 13.1 °C, attributed to the diffraction peak of the conjugated aromatic ring in the in-plane repeating unit (Jin et al., 2019). As for the XRD patterns of $\text{NiCo}_2\text{S}_4/\text{g-C}_3\text{N}_4$ composites contain the peaks of both $\text{g-C}_3\text{N}_4$ and NiCo_2S_4 , the diffraction peaks at 2 theta of 31.8°, 38.3°, 47.2°, 50.7° and 55.3° corresponded to the characteristic diffraction peak of Composite metal sulfides NiCo_2S_4 and the reflections at 2 theta of 13.1° and 27.8° were assigned to $\text{g-C}_3\text{N}_4$, which directly proved the successful loading of NiCo_2S_4 on $\text{g-C}_3\text{N}_4$. Due to the low content or low crystallinity of Co, Ni and S elements, there was low intensity of diffraction peaks corresponding to transition metal sulfur compounds in the composites was observed by XRD analysis.

The surface chemical state and elemental composition of $\text{NiCo}_2\text{S}_4/\text{g-C}_3\text{N}_4$ structure were analyzed by XPS. Fig. 2(b) shows the XPS spectra of the Co 2p region. 778.8 and 793.8 eV peaks were attributed to Co 2p_{3/2} and Co 2p_{1/2}, while Co 2p_{1/2} and Co 2p_{3/2} had sharp orbital splitting values above 15 eV, indicating that $\text{Co}^{2+}/\text{Co}^{3+}$ coexist on the surface of the $\text{NiCo}_2\text{S}_4/\text{g-C}_3\text{N}_4$ composite. In addition, the peaks at 782.1 eV

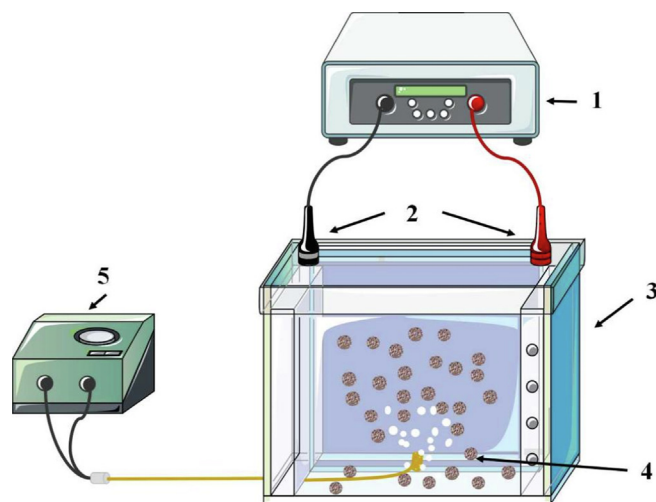


Fig. 1 Schematic of the three-dimensional electrochemical system. (1) power supply, (2) cathode plate and anode plate, (3) electrolytic cell, (4) particle electrodes, (5) aeration system.

and 798.3 eV were consistent with the Co-N bond and the oxidation state of Co (Wang et al., 2017a). Fig. 2(c) shows the Ni2p XPS spectrum of the NiCo₂S₄/g-C₃N₄. In the Ni 2p spectrum, the peaks at 853.3 and 874.8 eV belong to Ni²⁺ and the peaks at 856.9 and 880.0 eV belong to Ni³⁺. Meanwhile, the peaks at 862.2 and 882.4 eV belong to the corresponding satellite peaks (Jin et al., 2021). As shown in the Fig. 2(d), S 2p XPS spectra can be fitted to four peaks at 161.6, 162.8 eV, 168.9 eV, and 163.8 eV, corresponding to Ni-S bonds, Co-S bonds, satellite peaks, and the bond between metal and sulfur, indicating the presence of S²⁻ species (Li et al., 2020). The C 1s spectrum in Fig. 2(e) was fitted to two peaks. For NiCo₂S₄/g-C₃N₄, the two strong peaks for C1s are concentrated at 284.7 and 288.5 eV. These peaks were attributed to sp² carbon atoms in the N=C=N and to carbon species on the surface of g-C₃N₄ (Li et al., 2020). Similarly, The N 1s XPS spectra of NiCo₂S₄/g-C₃N₄ composites exhibit two main peaks at 399.2 eV and 400.7 eV in the Fig. 2(f), which assigned to the bond of Co-N and the peak of pyrrolic nitrogen. An earlier study reported that the presence of pyridine nitrogen facilitates the redox process (Teng et al., 2023). Finally, we also added the elemental distribution table of each element in NiCo₂S₄/g-C₃N₄ by XPS as shown in Table S1.

The morphology and microstructure of g-C₃N₄, NiCo₂S₄ and NiCo₂S₄/g-C₃N₄ composites were investigated by SEM and TEM. Fig. 3a-c show the SEM images of g-C₃N₄, NiCo₂S₄ and NiCo₂S₄/g-C₃N₄. The g-C₃N₄ shows irregular blocky particles that are loosely agglomerated, thus leading to the formation of some cavities due to their physical accumulation. NiCo₂S₄ particles are made up of layers of nanoflakes connected in a tightly packed manner. The flaky NiCo₂S₄ particles were found to be uniformly doped with granular g-C₃N₄ in NiCo₂S₄/g-C₃N₄, and a plated coating was formed on the surface of the compound. The transmission electron micrographs of g-C₃N₄, NiCo₂S₄ and NiCo₂S₄/g-C₃N₄ are shown in Fig. 3d-f. g-C₃N₄ has a lamellar thin nanosheet stacking composition with irregular morphology. Fig. 3d clearly reveals the irregular needle-like nanostructure of the NiCo₂S₄ sample. Fig. 3f shows that the NiCo₂S₄ nanorods are embedded in very thin sheets of g-C₃N₄. By SEM and TEM, we found that NiCo₂S₄/g-C₃N₄ is composed of porous g-C₃N₄ and NiCo₂S₄

uniformly doped, which has the advantages of both materials. g-C₃N₄ can be used not only as a catalyst but also as a catalytic carrier for NiCo₂S₄. NiCo₂S₄ as an active component that facilitates the electrocatalytic reaction.

3.2. Effect of parameters on quinoline removal

We examined the effect of reaction time on the COD removal efficiency as shown in Fig. 4(a). The degradation efficiency of quinoline gradually increased with the increase of time. The degradation efficiency stabilized at 95.6% when the reaction time was 30 min. In the 3D-EF, the high organic component content of the quinoline wastewater at the beginning of the reaction was easily removed by the oxidation reaction. After 30 min, the content of organic matter decreases and the presence of refractory intermediates led to a decrease in COD removal efficiency. Therefore, the optimum reaction time of 30 min was chosen for the subsequent experiments.

In this study, the effect of catalyst dosage (30–70 g/L) on quinoline COD removal efficiency was explored. As seen in Fig. 4(b), the COD degradation rate increased from 61.6% to 95.6% within 30 min when the catalyst dosage was increased from 30 g/L to 60 g/L after adding NiCo₂S₄/g-C₃N₄ to the reaction system. However, when the catalyst dosage continued to increase from 60 g/L to 70 g/L, the degradation rate of quinoline did not change greatly and even decreased. On the one hand, when the dosage of NiCo₂S₄/g-C₃N₄ was increased from 30 to 60 g/L, the increase of cobalt-nickel content leads to an increase of active sites, which results in Fenton-like reaction. Meanwhile, the further increase of catalyst dosage led to the generation of a large amount of ·OH radicals, which opens the ring of quinoline due to the strong oxidation of ·OH radicals, thus causing the increase of COD removal efficiency (Zhang et al., 2018b). On the other hand, a large number of ·OH radicals reacted with each other internally leading to rapid quenching of the radicals, which caused a decrease in degradation efficiency (Wang et al., 2017b). Based on the above analysis, the catalyst dosage was set at 60 g/L in this study.

Considering the significant effect of pH on the Fenton reaction process, batch degradation experiments were conducted at different initial pH values, and the results are shown in Fig. 4

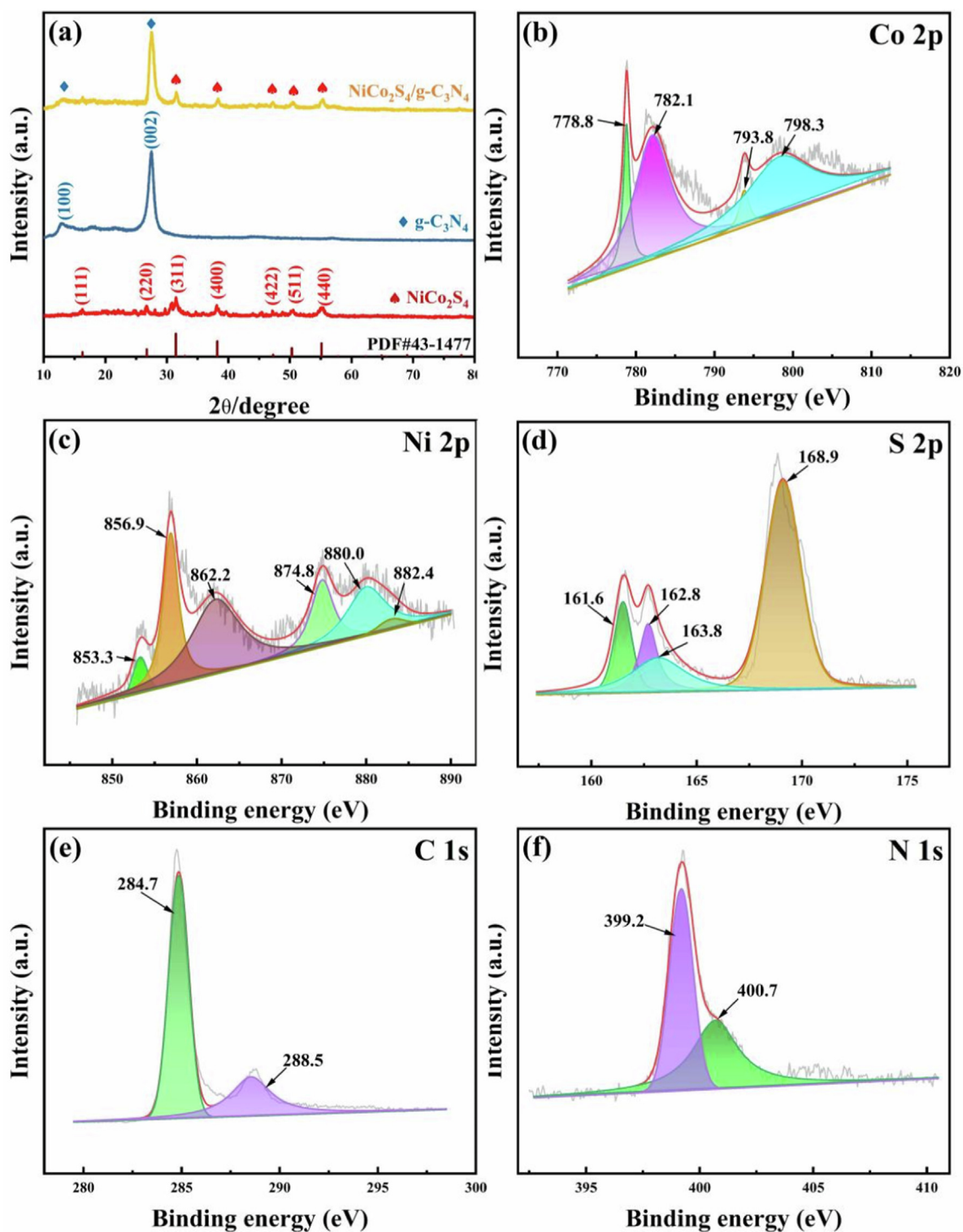


Fig. 2 XRD pattern of the samples: (a) NiCo_2S_4 , $\text{g-C}_3\text{N}_4$ and $\text{NiCo}_2\text{S}_4/\text{g-C}_3\text{N}_4$. XPS spectra of $\text{NiCo}_2\text{S}_4/\text{g-C}_3\text{N}_4$: (b) Co 2p; (c) Ni 2p; (d) S 2p; (e) C 1s; (f) N 1s.

(c). The removal rate of quinoline increased from 87.2% to 95.5% when the pH was increased from 2.0 to 3.0 and decreased from 83.6% to 57.5% when the pH was increased from 4.0 to 6.0 within 30 min. This indicated that the pH of the solution had an important effect on the degradation reaction rate. When the pH was above 4, the H_2O_2 generated in situ at the cathode tended to decompose into O_2 instead

of generating $\cdot\text{OH}$ radicals with catalytic oxidation ability. In general, the optimal pH of most electro-Fenton catalysts was about 3.0 (Zhong and Wang 2016), while $\text{NiCo}_2\text{S}_4/\text{g-C}_3\text{N}_4$ can effectively degrade quinoline in the pH range of 2.0–4.0, indicating that the catalyst can show excellent catalytic ability over a wide pH range.

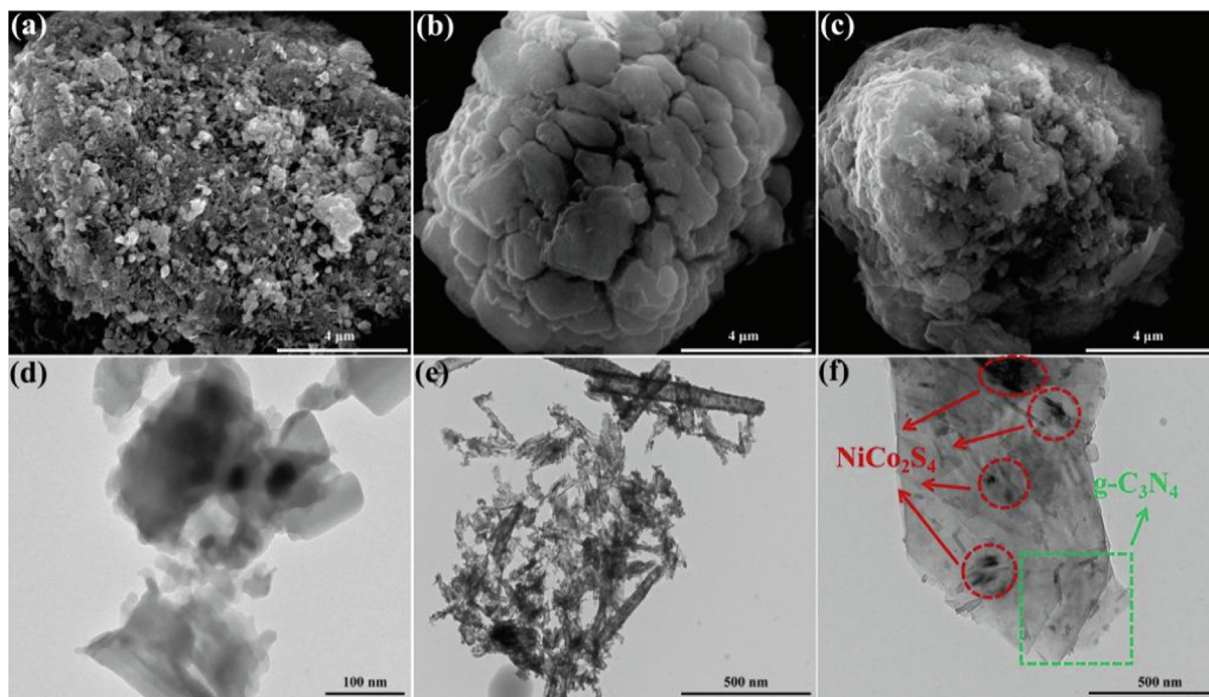


Fig. 3 Scanning electron microscopy images of (a) g-C₃N₄, (b) NiCo₂S₄, (c) NiCo₂S₄/g-C₃N₄. Transmission electron microscopy images of (d) g-C₃N₄, (e) NiCo₂S₄, (f) NiCo₂S₄/g-C₃N₄.

The effect of H₂O₂ addition on quinoline removal efficiency was shown in Fig. 7(d). As the H₂O₂ addition increased, the rate of quinoline removal increased after 30 min reaction. However, when the H₂O₂ concentration reached 96.4 mmol/L, the rate of COD removal declined instead. H₂O₂ is the main part of Fenton reaction and Fenton-like reaction. The augment of H₂O₂ concentration induced more •OH generated by particles, effectively removing the pollutants in short time. However, excessive H₂O₂ can inhibit the formation of •OH and react with •OH to generate HO₂ free radicals with low oxidation activity, which weakens the oxidation ability of the reaction system (Ghosh et al., 2011). In the constructed 3D-EF system, the optimal H₂O₂ concentration of 67.6 mmol/L was obtained in the tests.

As can be seen from Fig. 4(e), conductivity had an important effect on the quinoline COD removal rate. When NaCl was added as electrolyte, the lowest COD removal rate (68.2%) was observed with a conductivity of 6.5 ms/cm; and the highest COD removal rate (95.6%) was observed with a conductivity of 12.1 ms/cm. The electrolyte was injected in a certain concentration range, which helped to improve the quinoline degradation. With the increase of electrolyte concentration, the transfer of positive and negative ions in the solution was accelerated, and the efficiency of current transfer was improved. However, too high a concentration of electrolyte can affect the Fenton and Fenton-like reactions and hinder the chemical reactions on the catalyst and electrode surfaces (Hong et al., 2021). A comprehensive analysis suggested that a conductivity of 12.1 ms/cm (1.5 g/L NaCl) was more appropriate.

The current directly affects the efficiency of cathode H₂O₂ production and a suitable current needs to be selected (Behrouzeh et al., 2022). As shown in Fig. 4(f), when the current was increased from 2 A to 5 A for 30 min, the quinoline

COD removal rate increased from 60.4% to 95.6%. The degradation efficiency of quinoline decreased by 4.7% after 30 min by continuing to increase the current to 6 A. This was because the increase of current can make the cathode produce a large amount of H₂O₂, while the oxygen and hydrogen precipitation side reaction occurs to produce micro bubbles to accelerate the reaction. However, excess hydrogen peroxide can react with hydroxyl radicals and consume them resulting in low degradation efficiency (Tao et al., 2008). At the same time, too high a current has a high energy consumption, so the current was optimal at 5A.

When the reaction time was 30 min, the catalyst particle dosage was 60 g/L, the pH value was 3, the conductivity was 12.1 ms/cm, the current was 5A and the H₂O₂ concentration was 67.6 mmol/L as the optimal reaction conditions for 3D-EF. The removal efficiency of different catalysts for quinoline COD was investigated under optimal conditions. It can be seen that when there was no catalyst, the COD removal rate of quinoline reached 61.2% after 30 min. It shows that the degradation of quinoline was mainly caused by the Fenton reaction between the iron ions precipitated from the anode iron plate and the H₂O₂ produced at the cathode or additionally added. g-C₃N₄ was widely used as a photocatalyst for wastewater treatment, while the porous structure provides a large number of active sites, but the COD removal can only be improved by 8.4% within 30 min, indicating that g-C₃N₄ does not play a major role in the whole catalytic system, but only plays the role of a carrier. NiCo₂S₄ can improve COD removal about 17.4% within 30 min and can be used as the active component of catalyst. The main reason was that Co and Ni can generate •OH in Fenton-like reactions on the surface of catalytic particles, while the introduction of sulfur elements can increase the transfer of electrons to speed up the reaction. The NiCo₂S₄/g-C₃N₄ prepared by mixing the above two components can be

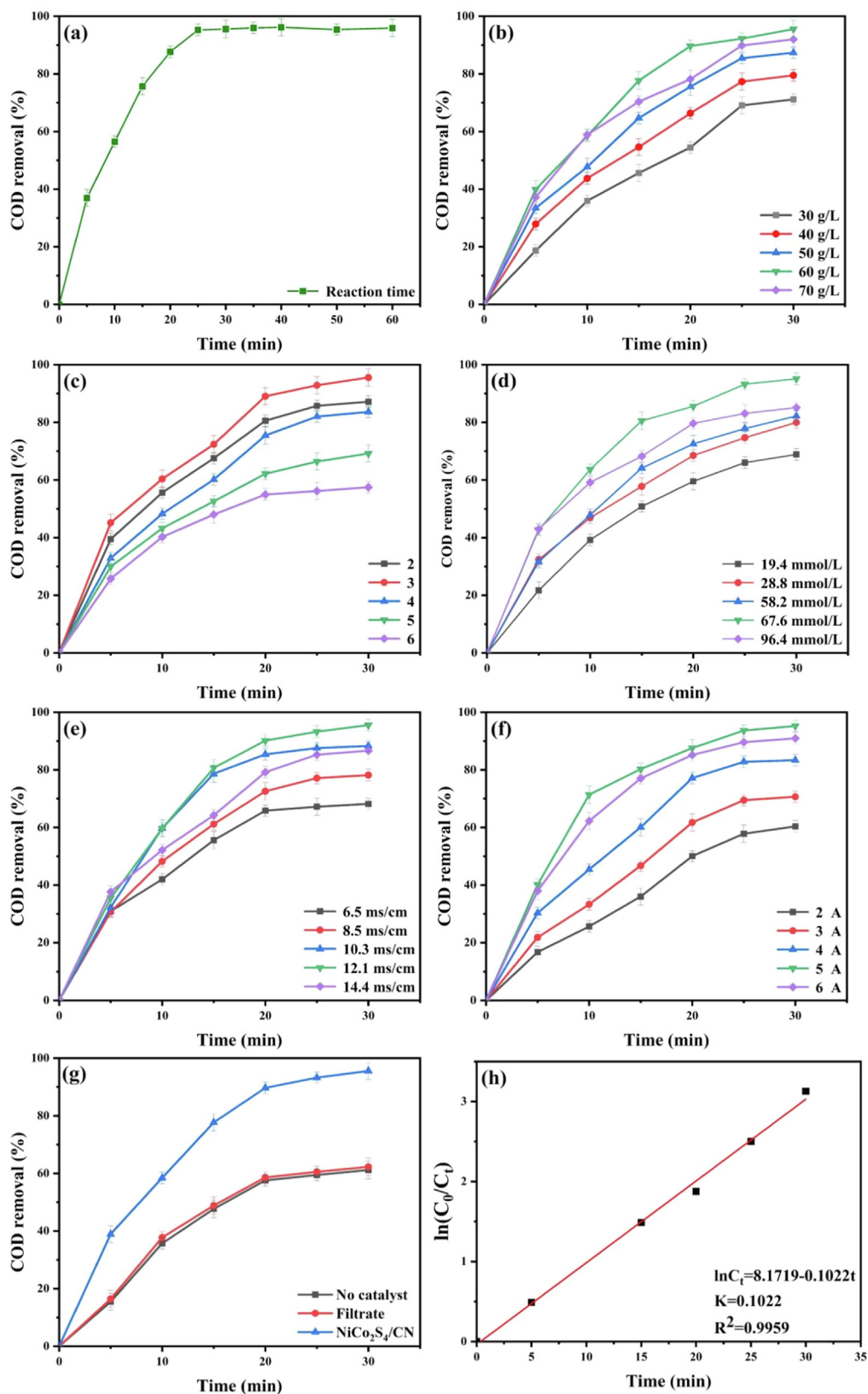


Fig. 4 Effects of operational parameters on COD removal rate: (a) reaction time; (b) electrode dosage; (c) pH; (d) H₂O₂ concentration; (e) electrical conductivity; (f) current; (g) Removal of quinoline COD by different catalysts. (h) Linear dependence of first-order reaction based on COD.

used as a non-homogeneous class of Fenton catalysts with better catalytic degradation effect, which can enhance about 30% COD removal, indicating a strong synergistic effect between $\text{g-C}_3\text{N}_4$ and NiCo_2S_4 (Fig. 4(g)).

3.3. Kinetics analysis of COD degradation

The study of the reaction kinetics of degraded quinoline was important to improve the degradation rate of the whole reaction process and to optimize the reaction conditions (Zhang et al., 2021). The quinoline COD removal efficiency was the highest at a reaction time of 30 min, a $\text{NiCo}_2\text{S}_4/\text{g-C}_3\text{N}_4$ dosage of 60 g/L, a pH of 3, a conductivity of 12.1 ms/cm, and a current of 5A. The relationship between COD of quinoline solution and reaction time under optimal conditions was shown in Table S2. The first-order kinetic constant k was determined to be 0.1022 min^{-1} by the first-order kinetic model (Eq. (1)). In addition, the correlation coefficients R^2 of the degradation processes are all close to 1, which further demonstrates that the present reaction process was consistent with the first-order kinetic model. The above relationships are shown in Fig. 4(h).

$$\ln(C_0/C_t) = K_1t \quad (1)$$

3.4. Investigation on the material stability

The stability of the catalyst was tested using continuous catalytic experiments. The stability of the catalyst was investigated when the $\text{NiCo}_2\text{S}_4/\text{g-C}_3\text{N}_4$ dosage was 60 g/L, pH was 3, conductivity was 12.1 ms/cm and current was 5A as shown in Fig. S1(a). The COD removal rate of quinoline reached more than 95% in the first five days of use, and after 25 days of repeated use, the COD removal rate of quinoline still reached more than 85%, and the catalytic performance remained basically unchanged, which indicated that the stability of the catalyst was good. In order to investigate the leaching of metal ions from the catalyst, the catalytic properties of the filtrate after the reaction were investigated. This was done as follows: $\text{NiCo}_2\text{S}_4/\text{g-C}_3\text{N}_4$ was filtered out, its filtrate was collected, and the filtrate was heated to 50°C to remove H_2O_2 from the solution, which was used as a solvent to still prepare a 1.5 g/L quinoline solution. The degradation rate of quinoline was investigated when the reaction time, pH, conductivity, and current were all optimal. We compare the differences between the three cases of no catalyst addition, filtrate addition, and $\text{NiCo}_2\text{S}_4/\text{g-C}_3\text{N}_4$ addition as shown in Fig. S1(b). As can be seen from the figure, the COD removal of the quinoline solution prepared from the filtrate was found to be almost unchanged compared with that without the addition of catalyst, indicating that the Co, Ni was almost not leached out and the leached Co, Ni homogeneous Fenton had almost no effect in the catalytic reaction. It was worth noting that the COD removal of the quinoline solution prepared from the filtrate was mainly due to the Fenton reaction between the iron ions leached from the anode and the hydrogen peroxide produced by the cathode, which generates $\cdot\text{OH}$ and thus reduces the quinoline COD. In addition, the quantitative analysis of metal elements by XRF to indirectly infer metal ion leaching is shown in Table S3. It showed the content of the main components of $\text{NiCo}_2\text{S}_4/\text{g-C}_3\text{N}_4$ particle electrodes and the

changes in the components after the reaction. Before the reaction, the contents in the active ingredients, i.e., Ni and Co in $\text{NiCo}_2\text{S}_4/\text{g-C}_3\text{N}_4$ particles were 5.35% and 7.87%, respectively. After 25 days, the corresponding contents of the active ingredients were reduced to 5.02% and 7.61%. In summary, there was less metal ion leaching from the particles and the catalyst had good stability and reusability.

3.5. Catalytic mechanism

In order to verify that $\cdot\text{OH}$ was the active substance in the process of carrying out the electro-Fenton catalytic reaction, the catalytic reaction was tested by EPR using DMPO as a radical trapping agent, and the results are shown in Fig. 5(a). The presence of four peaks with 1:2:2:1 within the EPR spectrum can be seen, which shows that $\cdot\text{OH}$ was indeed the main reactive group in the catalytic reaction process (Chen et al., 2022b). In addition, *tert*-butanol was added to 3D-EF and used as a free radical scavenger to capture $\cdot\text{OH}$, and the results are shown in Fig. 5(b). It can be seen that the system with the addition of *tert*-butanol showed a significant decrease in the quinoline COD removal rate. When the concentration of *tert*-butanol was 5.00 mmol/L, the COD removal rate only reached 51.4% after 30 min, which may be due to the capture of $\cdot\text{OH}$ by *tert*-butanol, making the COD decrease.

The EPR test identified $\cdot\text{OH}$ as the main reactive group in the electro-Fenton process. In the radical scavenging experiments, the addition of *tert*-butanol led to a decrease in the COD removal rate of the catalytic system, which also supports the view that $\cdot\text{OH}$ is the main reactive group in the catalytic process (Peng et al., 2017). In addition, the catalytic experiments of the filtrate showed that Co^{2+} , Ni^{2+} leached from the particle electrode did not contribute to the catalytic process, and it could be determined that $\text{NiCo}_2\text{S}_4/\text{g-C}_3\text{N}_4$ was the main active part in the catalytic reaction. The 3D-EF system simultaneously occurs in Fenton and Fenton-like reactions. A typical Fenton reaction was as follows. Firstly, the anode $\text{Fe}(0)$ was oxidized to $\text{Fe}(\text{II})$ under the action of current, while Fe^{2+} leached from the anode plate (Eqs. (2) and (3)). Subsequently, $\text{Fe}(\text{II})$ in the anode plate and Fe^{2+} in the solution are reacted with H_2O_2 generated from the cathode iron plate in non-homogeneous and homogeneous Fenton reactions, respectively (Eqs. (4) and (5)). In addition the typical Fenton-like reactions was as follows. The $\text{Co}(\text{II})$ and $\text{Ni}(\text{II})$ on catalytic particles were reacted with H_2O_2 produces $\cdot\text{OH}$ (Eqs. (6) and (7)). Subsequently, $\text{Co}(\text{III})$ and $\text{Ni}(\text{III})$ gaining electrons in solution. They were reduced to $\text{Co}(\text{II})$ and $\text{Ni}(\text{II})$ and adsorbed on $\text{NiCo}_2\text{S}_4/\text{g-C}_3\text{N}_4$ particles (Eqs. (8) and (9)). According to the XPS analysis of the obtained $\text{NiCo}_2\text{S}_4/\text{g-C}_3\text{N}_4$ particles, the catalytic particles contain S^{2-} . S^{2-} can accelerate the transition of metal ions from higher to lower valence states, and the generated $\text{Co}(\text{III})$ and $\text{Ni}(\text{III})$ can be rapidly generated from $\text{Co}(\text{II})$ and $\text{Ni}(\text{II})$ after electron transfer by S^{2-} on the surface of $\text{NiCo}_2\text{S}_4/\text{g-C}_3\text{N}_4$ particles (Eq. (10)) (Li et al., 2020). $\text{Co}(\text{II})/\text{Co}(\text{III})$ and $\text{Ni}(\text{II})/\text{Ni}(\text{III})$ on the surface of the particle electrode were continuously oxidized to remove contaminants in a reversible cycle. Finally, quinoline molecules were rapidly mineralized to small molecules (Eq. (11)) under the combined action of $\cdot\text{OH}$ on the surface of anode, $\cdot\text{OH}$ on the surface of $\text{NiCo}_2\text{S}_4/\text{g-C}_3\text{N}_4$ particles and $\cdot\text{OH}$ in solution, as shown in Fig. 6. The possible catalytic

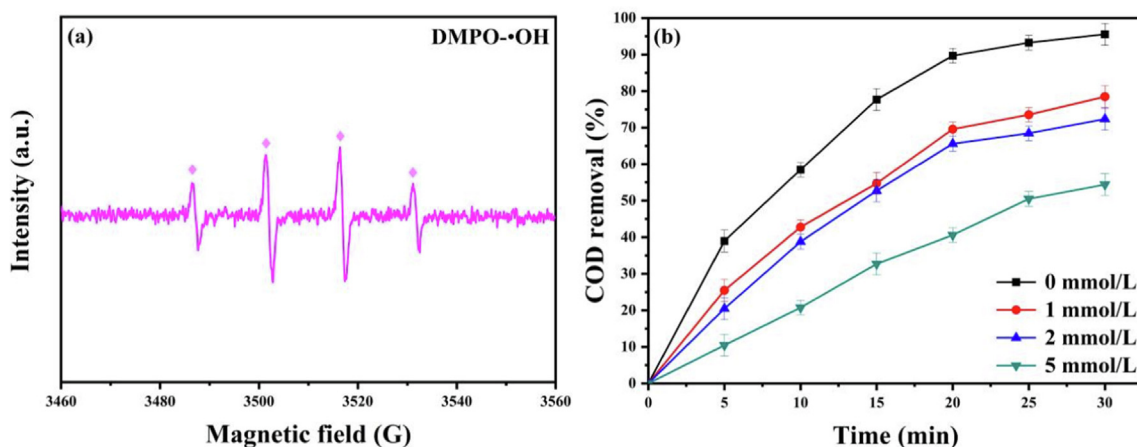
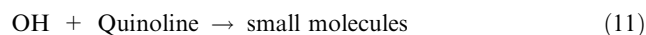
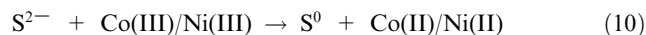
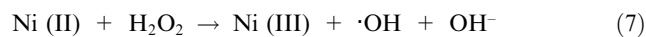
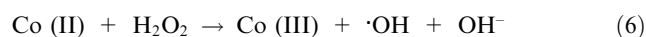
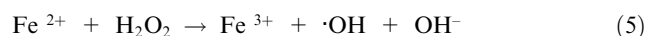
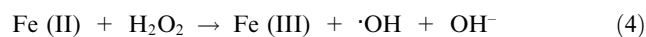


Fig. 5 (a) EPR detection spectra; (b) Effect of *tert*-butanol dosage on the rate of the COD removal.

mechanism of $\text{NiCo}_2\text{S}_4/\text{g-C}_3\text{N}_4$ as a Fenton-like catalyst in the 3D-EF system was speculated as follows.



3.6. Degradation pathways

The by-products generated by quinoline degradation in the 3D-EF system were analyzed by HPLC-MS as shown in Figs. S2 and S3 of the Supplementary Materials, and the possible structures of the products were shown in Table 1. Due to the strong oxidation of hydroxyl radicals, addition reactions and substitution reactions mainly occur in the degradation of quinoline molecules. We inferred two possible degradation pathways (Fig. 7). In pathway 1, the 8-position on the quinoline benzene ring was hydroxylated to form quinolin-8-ol, and the pyridine ring was not broken. The addition of $\cdot\text{OH}$ at the 8-position and 5-position to form quinoline-5,8-diol, and subsequent continued oxidation to quinoline-5,8-dione (Chen et al., 2022a). The benzene ring in the quinoline molecule was broken due to oxidation by the $\cdot\text{OH}$ generated on the surface of $\text{NiCo}_2\text{S}_4/\text{g-C}_3\text{N}_4$ particles and the electrodes to form 3-formylpicolinic acid, picolinic acid, pyridine. Finally, $\cdot\text{OH}$ continue to attack the pyridine ring to break the ring and form small molecules. Quinoline may also be added to $\cdot\text{OH}$ at the 2-position as shown in pathway 2 to form quinolin-2-ol, which was then oxidized to quinolin-2(1H)-one. The introduction of oxygens at the 2-position led to an increase in the charge density at the 3-position of the pyridine ring, which makes it easy for electrophilic reactions and ring-opening reactions at the 2-position to 3-position to occur (Jing et al., 2012). After ring

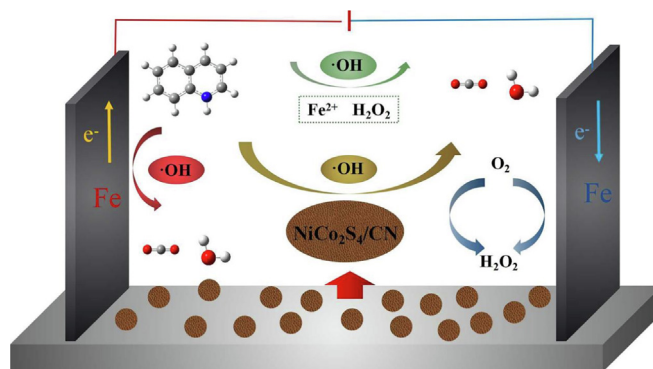


Fig. 6 Proposed catalytic mechanism of 3D-EF system.

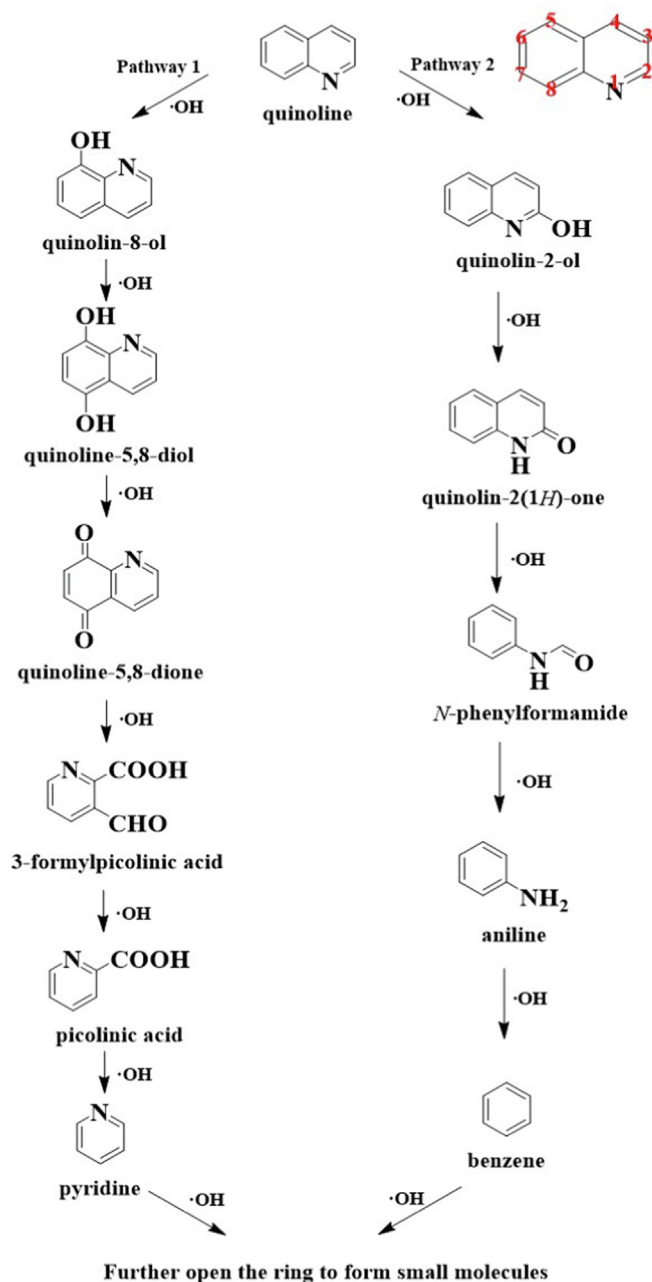


Fig. 7 Possible degradation pathways of quinoline in 3D-EF system.

opening, intermediate products such as *N*-phenylformamide, aniline and benzene were formed, which are eventually completely mineralized into small molecules.

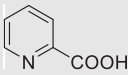
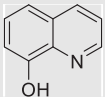
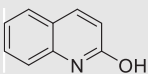
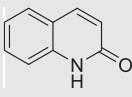
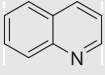
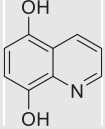
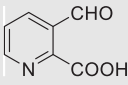
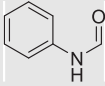
In a previous study by our group, the degradation rate of quinoline using Fe-Co-Ni-P/g-C₃N₄ particle electrode was 90.95%. Four intermediates were found by HPLC in addition to quinoline with a minimum relative molecular mass of 133.1 were 2,3-pyridinedicarboxyaldehyde and (Z)-3-phenylprop-2-en-1-amine, respectively (Chen et al., 2019). In this study, the removal rate of quinoline reached about 95%, and eight intermediates were found by HPLC in addition to quinoline, with a minimum relative molecular mass of 79, 124 corresponding to benzene and picolinic acid, respectively. When compared in terms of degradation efficiency and relative molecular mass, NiCo₂S₄/g-C₃N₄ showed higher degradation efficiency and

better mineralization of quinoline. The possible reason for this result is that the electronegativity of sulfur is greater than that of phosphorus, and sulfur has a greater ability to attract electrons, which accelerates the transfer of electrons in Fenton-like reactions, increasing the rate of chemical reactions and producing more hydroxyl radicals.

3.7. Biochemical analysis of wastewater

COD and BOD are the two commonly used indicators in the biological treatment of wastewater, and BOD/COD is commonly used to evaluate the biochemical properties of wastewater (Oladipo et al., 2017). When $B/C < 0.2$ means not suitable for biochemical; $0.2 < B/C < 0.3$ means difficult to biochemical; $0.3 < B/C < 0.45$ means can be biochemical; $B/C > 0.45$

Table 1 Possible major intermediates in the quinoline degradation process.

Compound	[M + H] ⁺ (m/z)	Chemical structure
Benzene	79	
Picolinic acid	124	
Quinolin-8-ol	146	
Quinolin-2-ol	146	
Quinolin-2(1H)-one	146	
Quinoline	130	
Quinoline-5,8-diol	162	
3-Formylpicolinic acid	152	
N-phenylformamide	122	

means good biochemical. As shown in Table S4, the COD of quinoline wastewater decreased from 3540 mg/L to 155 mg/L after 3D-EF treatment, and the removal rate was 95.6%, indicating that the 3D-EF method can effectively remove most organic pollutants from quinoline wastewater. The BOD could be reduced from 885 mg/L to 72 mg/L, while the B/C ratio increased from 0.24 to 0.46, which showed that the biochemical properties of the wastewater were obviously improved and created good conditions for subsequent biochemical treatment. Finally, we also studied the toxicological part of the data for quinolines and their degradation products as shown in Table S5 of the Supplementary Materials.

4. Conclusion

In this study, NiCo₂S₄ nanoparticles were prepared and doped NiCo₂S₄/g-C₃N₄ particle catalysts were prepared with g-C₃N₄ as the carrier. NiCo₂S₄/g-C₃N₄ exhibited excellent Fenton-like catalytic activity and cyclic stability. The degradation rate of high concentration quinoline (COD = 3540 mg/L) was 95.6% within 30 min under optimal conditions of 3D-EF. Kinetic analysis showed that the COD degradation of quinoline solutions by the 3D-EF followed first-order kinetic model. The excellent reactivity of the catalyst can be attributed to the large amount of low valence metal ions (Fe²⁺, CO(II), Ni(II)) and the syn-

ergistic interaction between NiCo₂S₄ and g-C₃N₄. EPR and radical scavenging tests showed that hydroxyl radicals play a major role in the degradation of quinoline. The degradation intermediates were detected by HPLC-MS, and two main mechanisms and pathways of quinoline degradation were proposed. The degradation of quinoline by the 3D-EF system showed a significant tendency to reduce the toxicity level by BOD/COD values and partial ecotoxicity data of the degradation products. This study provided a method for the removal of quinoline wastewater by the addition of transition metal sulfide catalysts.

CRedit authorship contribution statement

Boding Zhang: Supervision, Writing – review & editing. **Jun Chen:** Methodology, Investigation. **Bingxing Wang:** Writing – review & editing. **Chengxing Cui:** Data curation, Formal analysis. **Songlin Wang:** Conceptualization, Supervision. **Jichao Wang:** Resources, Formal analysis. **Wenlong Zhang:** Validation, Writing – review & editing.

Declaration of Competing Interest

The authors declare that they have no known competing financial interests or personal relationships that could have appeared to influence the work reported in this paper.

Acknowledgments

This research was supported by the National Natural Science Foundation of China (No. 51802082), and by the Program for Science & Technology Innovation Talents in Universities of Henan Province (21HATITO16). The authors thank both projects for their support.

Appendix A. Supplementary material

Supplementary material to this article can be found online at <https://doi.org/10.1016/j.arabjc.2023.104983>.

References

- Barhouni, N., Olvera-Vargas, H., Oturan, N., et al, 2017. Kinetics of oxidative degradation/mineralization pathways of the antibiotic tetracycline by the novel heterogeneous electro-Fenton process with solid catalyst chalcocopyrite. Appl. Catal. B 209, 637–647. <https://doi.org/10.1016/j.apcatb.2017.03.034>.
- Behrouzeh, M., Parivazh, M.M., Danesh, E., et al, 2022. Application of Photo-Fenton, Electro-Fenton, and Photo-Electro-Fenton processes for the treatment of DMSO and DMAC wastewaters. Arab. J. Chem. 15. <https://doi.org/10.1016/j.arabjc.2022.104229> 104229.
- Bhaumik, M., Maity, A., Brink, H.G., 2022. Metallic nickel nanoparticles supported polyaniline nanotubes as heterogeneous Fenton-like catalyst for the degradation of brilliant green dye in aqueous solution. J. Colloid Interface Sci. 2022, 408–420. <https://doi.org/10.1016/j.jcis.2021.11.181>.
- Chaugule, A.A., Mane, V.S., Bandal, H.A., et al, 2019. Ionic Liquid-derived Co₃O₄-N/S-doped Carbon Catalysts for the enhanced water oxidation. ACS Sustain. Chem. Eng. 7, 14889–14898. <https://doi.org/10.1021/acssuschemeng.9b02997>.
- Chen, Z., Bi, S., Zhao, G., et al, 2020. Enhanced degradation of triclosan by cobalt manganese spinel-type oxide activated peroxy-monosulfate oxidation process via sulfate radicals and singlet oxygen: Mechanisms and intermediates identification. Sci. Total

- Environ. 711,. <https://doi.org/10.1016/j.scitotenv.2019.134715> 134715.
- Chen, R., Wang, P., Chen, J., et al, 2019. Synergetic effect of MoS₂ and MXene on the enhanced H₂ evolution performance of CdS under visible light irradiation. *Appl. Surf. Sci.* 473, 11–19. <https://doi.org/10.1016/j.apsusc.2018.12.071>.
- Chen, J., Zhang, B., Wang, B., et al, 2022a. Enhanced degradation of quinoline in three-dimensional electro-Fenton system using catalytic Fe-Co-Ni-P/g-C₃N₄ particles. *Int. J. Electrochem. Sci.* 12, 221296. <https://doi.org/10.20964/2022.12.109>.
- Chen, J., Zhang, B., Wang, B., et al, 2022b. Heterogeneous electro-Fenton using three-dimension Fe-Co-Bi/kaolin particle electrodes for degradation of quinoline in wastewater. *Environ. Sci. Pollut. Res.* 22, 22232–22234. <https://doi.org/10.1007/s11356-022-22232-4>.
- Feng, M., Wang, Z., Dionysiou, D.D., et al, 2018. Metal-mediated oxidation of fluoroquinolone antibiotics in water: A review on kinetics, transformation products, and toxicity assessment. *J. Hazard. Mater.* 344, 1136–1154. <https://doi.org/10.1016/j.jhazmat.2017.08.067>.
- Ghosh, P., Samanta, A.N., Ray, S., 2011. Reduction of COD and removal of Zn²⁺ from rayon industry wastewater by combined electro-Fenton treatment and chemical precipitation. *Desalination* 266, 213–217. <https://doi.org/10.1016/j.desal.2010.08.029>.
- Hong, L., Yang, H., Cheng, J., et al, 2021. Three-dimensional particle electrode system treatment of organic wastewater: A general review based on patents. *J. Clean. Prod.* 308,. <https://doi.org/10.1016/j.jclepro.2021.127324> 127324.
- Hou, B., Ren, B., Deng, R., et al, 2017. Three-dimensional electro-Fenton oxidation of N-heterocyclic compounds with a novel catalytic particle electrode: high activity, wide pH range and catalytic mechanism. *RSC Adv.* 7, 15455–15462. <https://doi.org/10.1039/C7RA00361G>.
- Jiang, D., Li, J., Xing, C., et al, 2015. Two-Dimensional CaIn₂S₄/g-C₃N₄ Heterojunction Nanocomposite with Enhanced Visible-Light Photocatalytic Activities: Interfacial Engineering and Mechanism Insight. *JACS Appl. Mater. Interfaces* 7, 19234–19242. <https://doi.org/10.1021/acsami.5b05118>.
- Jin, D., Li, Z., Wang, Z., 2021. Hierarchical NiCo₂O₄ and NiCo₂S₄ nanomaterials as electrocatalysts for methanol oxidation reaction. *Int. J. Hydrogen Energy* 46. <https://doi.org/10.1016/j.ijhydene.2021.06.226>.
- Jin, C., Xu, C., Chang, W., et al, 2019. Bimetallic phosphide NiCoP anchored g-C₃N₄ nanosheets for efficient photocatalytic H₂ evolution. *J. Alloy. Compd.* 803, 205–215. <https://doi.org/10.1016/j.jallcom.2019.06.252>.
- Jing, J., Li, W., Boyd, A., et al, 2012. Photocatalytic degradation of quinoline in aqueous TiO₂ suspension. *J. Hazard. Mater.* 237–238, 247–255. <https://doi.org/10.1016/j.jhazmat.2012.08.037>.
- Li, Y., Li, J., Pana, Y., et al, 2020. Peroxymonosulfate activation on FeCo₂S₄ modified g-C₃N₄ (FeCo₂S₄-g-C₃N₄): Mechanism of singlet oxygen evolution for nonradical efficient degradation of sulfamethoxazole. *Chem. Eng. J.* 384. <https://doi.org/10.1016/j.cej.2019.123361>.
- Li, Y., Dong, H., Li, L., et al, 2021b. Recent advances in waste water treatment through transition metal sulfides-base d advanced oxidation processes. *Water Res.* 192,. <https://doi.org/10.1016/j.watres.2021.116850> 116850.
- Li, M., Qin, X., Cui, J., et al, 2021a. Three-dimensional Electro-Fenton degradation for fulvic acids with Cu-Fe bimetallic aerogel-like carbon as particle electrode and catalyst: electrode preparation, operation parameter optimization and mechanism. *J. Environ. Chem. Eng.* 9,. <https://doi.org/10.1016/j.jece.2021.105573> 105573.
- Lin, X., Shih, K., Chen, J., et al, 2019. Insight into flower-like greigitze-based peroxydisulfate activation for effective bisphenol a abatement: Performance and electron transfer mechanism. *Chem. Eng. J.* 391,. <https://doi.org/10.1016/j.cej.2019.123558> 123558.
- Liu, Y., Ma, Y., Wan, J., et al, 2021. Electrocatalytic oxidation of ciprofloxacin by Co-Ce-Zr/γ-Al₂O₃ three-dimensional particle electrode. *Environ. Sci. Pollut. Res.* 28, 43815–43830. <https://doi.org/10.1007/s11356-021-13547-9>.
- Long, Y., Feng, Y., Li, X., et al, 2018. Removal of Diclofenac by Three-Dimensional Electro-Fenton-Persulfate (3D Electro-Fenton-PS). *Chemosphere* 219, 1024–1031. <https://doi.org/10.1016/j.chemosphere.2018.12.054>.
- Luo, Y., Yue, X., Wei, P., et al, 2020. A state-of-the-art review of quinoline degradation and technical bottlenecks. *Sci. Total Environ.* 747,. <https://doi.org/10.1016/j.scitotenv.2020.141136> 141136.
- Masekela, D., Hintsho-Mbita, N.C., Sam, S., et al, 2023. Application of BaTiO₃-based catalysts for piezocatalytic, photocatalytic and piezophotocatalytic degradation of organic pollutants and bacterial disinfection in wastewater: A comprehensive review. *Arab. J. Chem.* 16. <https://doi.org/10.1016/j.arabjc.2022.104473>.
- Molaei, P., Rahimi-Moghadam, F., 2021. Porous g-C₃N₄ nanosheets through facile thermal polymerization of melamine in the air for photocatalyst application. *J. Mater. Sci.-Mater. Electron.* 32, 19655–19666. <https://doi.org/10.1007/s10854-021-06488-z>.
- Oladipo, A.A., Adeleye, O.J., Oladipo, A.S., et al, 2017. Bio-derived MgO nanopowders for BOD and COD reduction from tannery wastewater. *J. Water Process. Eng.* 16, 142–148. <https://doi.org/10.1016/j.jwpe.2017.01.003>.
- Peng, L., Liu, Z., Wang, X., et al, 2017. Enhanced decolorization of methyl orange in aqueous solution using iron-carbon micro-electrolysis activation of sodium persulfate. *Chemosphere* 180, 100–107. <https://doi.org/10.1016/j.chemosphere.2017.04.019>.
- Song, Z., Wang, M., Wang, Z., et al, 2019. Insights into Heteroatom-Doped Graphene for Catalytic Ozonation: Active Centers, Reactive Oxygen Species Evolution, and Catalytic Mechanism. *Environ. Sci. Tech.* 53, 5337–5348. <https://doi.org/10.1021/acs.est.9b01361>.
- Su, Y., Wang, Y., Xia, L., et al, 2022. 3D coral-like Fe doped NiCo₂S₄ cathode for stable high-efficiency photoelectrochemical tetracycline degradation and simultaneous energy recovery. *Chem. Eng. J.* 449,. <https://doi.org/10.1016/j.cej.2022.137867> 137864.
- Tao, Z., Li, Y., Jing, J., et al, 2008. Oxidation of 4-chlorophenol in a heterogeneous zero valent iron/H₂O₂ Fenton-like system: Kinetic, pathway and effect factors. *Sep. Purif. Technol.* 62, 551–558. <https://doi.org/10.1016/j.seppur.2008.03.008>.
- Teng, K., Tang, W., Qi, R., et al, 2023. Nitrogen-deficient g-C₃N₄ compounded with NiCo₂S₄ (NiCo₂S₄@ND-g-C₃N₄) as a bifunctional electrocatalyst for boosting the activity of Li-O₂ batteries. *Catal. Today* 409, 23–30. <https://doi.org/10.1016/j.cattod.2022.06.014>.
- Wang, J., Liu, C., Li, J., et al, 2017b. In-situ incorporation of iron-copper bimetallic particles in electrospun carbon nanofibers as an efficient Fenton catalyst. *Appl. Catal. B* 207, 316–325. <https://doi.org/10.1016/j.apcatb.2017.02.032>.
- Wang, D., Zhang, X., Du, Z., et al, 2017a. CoNi₂S₄ nanoparticles as highly efficient electrocatalysts for the hydrogen evolution reaction in alkaline media. *Int. J. Hydrogen Energy* 42. <https://doi.org/10.1016/j.ijhydene.2016.09.115>.
- Wang, C., Zhang, W., Fan, J., et al, 2021. S-scheme bimetallic sulfide ZnCo₂S₄/g-C₃N₄ heterojunction for photocatalytic H₂ evolution. *Ceram. Inter.* 7, 199. <https://doi.org/10.1016/j.ceramint.2021.07.199>.
- Xu, T., Long, Y., He, C., et al, 2021. Construction of dual-carbon-confined metal sulfide nanocrystals via bio-mimetic reactors enabling superior Fenton-like catalysis. *J. Mater. Chem. A* 9, 22994–23010. <https://doi.org/10.1039/D1TA04831G>.
- Yuan, R., Qin, Y., He, C., et al, 2023. Fe-Mn-Cu-Ce/Al₂O₃ as an efficient catalyst for catalytic ozonation of bio-treated coking wastewater: Characteristics, efficiency, and mechanism. *Arab. J. Chem.* 16. <https://doi.org/10.1016/j.arabjc.2022.104415>.
- Zhang, W., Xie, D., Li, X., Ye, W., et al, 2018a. Electrocatalytic removal of humic acid using cobalt-modified particle electrodes. *Appl. Catal. A Gen.* 559, 75–84. <https://doi.org/10.1016/j.apcata.2018.04.012>.

- Zhang, W., Chen, J., Wang, J., et al, 2021. Impact of Active Chlorines and $\bullet\text{OH}$ Radicals on Degradation of Quinoline Using the Bipolar Electro-Fenton Process. *Water* 13, 128. <https://doi.org/10.3390/w13020128>.
- Zhang, B., Hou, Y., Yu, Z., et al, 2018b. Three-dimensional electro-Fenton degradation of Rhodamine B with efficient Fe-Cu/kaolin particle electrodes: Electrodes optimization, kinetics, influencing factors and mechanism. *Sep. Purif. Technol.* 210, 60–68. <https://doi.org/10.1016/j.seppur.2018.07.084>.
- Zhao, J., Xian, Z., Hai, G., et al, 2021. CuO-doped Ce for catalytic wet peroxide oxidation degradation of quinoline wastewater under wide pH conditions. *J. Ind. Eng. Chem.* 105, 49–57. <https://doi.org/10.1016/j.jiec.2021.10.006>.
- Zhong, W., Wang, J., 2016. Degradation of sulfamethazine using $\text{Fe}_3\text{O}_4\text{-Mn}_3\text{O}_4$ /reduced graphene oxide hybrid as Fenton-like catalyst. *J. Hazard. Mater.* 324, 653. <https://doi.org/10.1016/j.jhazmat.2016.11.039>.